Preprint
UCRL-JC-135163

Spherical Harmonic Solutions to the 3D Kobayashi Benchmark Suite

P.N. Brown, B. Chang and U.R. Hanebutte

This article was submitted to
Physor 2000 American Nuclear Society Topical Meeting on
Advances in Reactor Physics and Mathematics and Computation
into the Next Millennium
Pittsburgh, PA
May 7-11, 2000

U.S. Department of Energy

Lawrence
Livermore
National
Laboratory

December 29, 1999

SPHERICAL HARMONIC SOLUTIONS TO THE 3D KOBAYASHI BENCHMARK SUITE

Peter N. Brown, Britton Chang and Ulf R. Hanebutte
Center for Applied Scientific Computing
Lawrence Livermore National Laboratory
P.O. Box 808 L-561
Livermore, CA

ABSTRACT

Spherical harmonic solutions of order 5, 9 and 21 on spatial grids containing up to 3.3 million cells are presented for the Kobayashi benchmark suite. This suite of three problems with simple geometry of pure absorber with large void region was proposed by Professor Kobayashi at an OECD/NEA meeting in 1996. Each of the three problems contains a source, a void and a shield region. Problem 1 can best be described as a box in a box problem, where a source region is surrounded by a square void region which itself is embedded in a square shield region. Problems 2 and 3 represent a shield with a void duct. Problem 2 having a straight and problem 3 a dog leg shaped duct. A pure absorber and a 50% scattering case are considered for each of the three problems. The solutions have been obtained with Ardra, a scalable, parallel neutron transport code developed at Lawrence Livermore National Laboratory (LLNL). The Ardra code takes advantage of a two-level parallelization strategy, which combines message passing between processing nodes and thread based parallelism amongst processors on each node. All calculations were performed on the IBM ASCI Blue-Pacific computer at LLNL.

1. INTRODUCTION

A benchmark suite of three problems with simple geometry of pure absorber with large void region was proposed by Kobayashi at an OECD/NEA meeting in 1996 (Kobayashi, 1997). In this paper we present benchmark results obtained by the parallel neutron transport code Ardra. For brevity, only a short overview of the Ardra code can be given here. Further details can be found in reference (Brown, 1999).

The steady state Boltzmann equation is solved by the Biconjugate Gradient Stabilized, BiCGSTAB, algorithm in conjunction with a sweeping algorithm. In the optically thick

regime, the Diffusion Synthetic Acceleration (DSA) preconditioner is used to accelerate the convergence of the solution. The (parallel) semicoarsening multigrid algorithm (SMG) in used to invert the DSA preconditioner.

A harmonic projection method has been developed and implemented within the code system, which allows users to obtain the quality of a spherical harmonics, or P_n solution, while exploiting the efficiency and better parallelizability of the S_n method.

The Ardra code exploits concurrency with respect to all phase space variables represented by direction, position and energy. The code takes advantage of a two-level parallelization strategy, which combines message passing between processing nodes and thread based parallelism amongst processors on each node. The parallel execution and interprocessor communication are performed by calls to MPI library routines, which insures portability among computing platforms. The node level parallelism is accomplished through the use of pthreads .The calculations were performed on the IBM ASCI Blue-Pacific Combined Technology Refresh (CTR) computer located at LLNL (LLNL, 1998).

2. RESULTS OF THE 3D KOBAYASHI BENCHMARK

The benchmark suite consists of three problems, each containing a source, a void and a shield region. Problem 1 can best be described as a box in a box problem, where a source region is surrounded by a square void region which itself is embedded in a square shield region. Problems 2 and 3 represent a shield with a void duct. The first one having a straight and the second a dog leg shaped duct. A pure absorber and a 50% scattering case are considered for each of the three problems. The cross section data and information regarding the source strenght for all problems are summarized in Table 1. All problems share common boundary conditions. On the bottom, left and front faces reflecting boundary conditions are prescribed, while vacuum conditions are given on the remaining three faces.

Performance date for the Ardra code on the ASCI Blue-Pacific CTR machine are given in Table 2 for spherical harmonic calculations of order 21. The ASCI Blue-Pacific CTR machine contains 336 nodes. Each node is a four way shared memory multiprocessor. Thus, the total number of processors is 1344. The table summarizes for each calculation the grid size, number of processing nodes and number of processors used, number of required iterations and achieved residual norm of the iterative solver, as well as the total solution time in seconds. The times are measured as wall clock time.

The benchmark requests scalar flux values at specific locations. Tables 3 through 8 summarizes scalar flux valued obtained with the Ardra code and compares these results to reference solution provided by Prof. Kobayashi (Sugimura,1998) for these specific locations. For the pure absorber cases, the reference solution is an analytic solution obtained by the University of Kyoto. For the 50% scattering cases, a solution obtained via the Monte Carlo method is given. Further, the relative error determined as the difference between the Ardra result and the reference solution divided by the reference solution is

given. The spatial discretizations are chosen such that the spatial points specified in the benchmark coincide with cell center points, while a near constant grid spacing is maintained.

The spherical harmonic solutions are obtained iteratively with a BiCGStab algorithm. Fig. 1, gives representatively the convergence history of the P_{21} calculation of problem 2i. The residual norm is sharply reduced during the first 10 iteration steps, while the convergence rate flattens noticeably thereafter.

While pointwise comparisons of scalar flux values at specific spatial locations are important for this benchmark, the quality of the solutions are better seen, when scalar flux distributions are visualized along surfaces away from the source region. Such visualizations are provided in Figs. 2 through 9. For each problem, scalar flux distributions along specific cut planes are shown with a logarithmic color scale (flux values which are negative or are less then 10^{-7} are set to 10^{-7}).

2.1 DISCUSSION OF PROBLEM 1

The geometry of problem 1 is a nested set of cubes. The three cubes have sides of lengths 10cm, 50cm and 100cm respectively. The cubes are arranged in such a way, that they share one common corner, which coincides with the origin of the coordinate system. The innermost cube represents the source region, which is surrounded by the void region. The remaining volume is the absorber.

For the pure absorber case, Table 3 compares spherical harmonic results of order 21 and discrete ordinates results of order S_{18} with the analytic solution provided by Kobayashi. The spherical harmonic solution of order 21 requires an angular discretization of 968 directions, while 360 discrete directions are necessary for S_{18}. For both calculations, the spatial discretization is a grid of 50x50x50 totaling 125,000 cells. Thus, the number of discretization points in phase space is 121 and 45 million points for P_{21} and S_{18} respectively. The superiority of the P_{21} solution over the high order dirscrete ordinate solution is best seen at the data points along the diagonal. There, the relative errors of the S_{18} solution are one to two orders of magnitude larger compared to the relative errors of the spherical harmonics solution. Fig. 2 presents the scalar flux distribution along the three vacuum boundary faces in a logarithmic color scale for the P_{21} calculation.

Sperical harmonic solutions of order 5 and 21 are presented in Table 4 for the case of 50% scattering. While a 50^3 spatial grid is used for the P_{21} calculation, a 150^3 spatial grid is applied for the P_5 calculation. The P_5 spherical harmonic approximation requires 72 discrete directions, thus the total number of discretization points is 243 and 121 million points for the P_5 and P_{21} calculation respectively. Comparing the relative errors for both calculations, one can conclude that for this particular problem the higher order spherical harmonic approximation on a less refined spatial grid produces a better result then the low order P_n approximation on a refined grid. The scalar flux distribution obtained with the P_5 calculation is given in Fig. 3.

2.2 DISCUSSION OF PROBLEM 2

The geometry of problem 2 can be seen in Fig. 4. The overall dimensions of the problem are 60cm x 100cm x 60cm. The source region is a cube of 10cm on a side located at the origin of the coordinate system. The void region is a straight duct with a cross section of 10cm x10cm. The remaining volume is the absorber.

Table 5 and 6 compare spherical harmonic results of order 5, 9 and 21 with the reference solution provided by Kobayashi. A spatial grid of 56x96x56 grid points is applied for all presented calculations. The total number of spatial cells is 301,056 and thus the number of discretization points in phase space is 21, 60 and 291 million points for P_5, P_9 and P_{21} respectively. For both cases the accuracy of the results improves with increasing spherical harmonic order.

Included with the results for Problem 2i is a solution obtained with P_1 (i.e. diffusion approximation). The scalar flux distribution obtained by the diffusion approximation is shown in Fig. 4. Comparing the diffusion results with the results obtained by a transport solver (Fig. 5) clearly shows the transport effects in this particular problem. For the diffusion solution, the flux distribution along the void duct is utterly wrong.

Flux distributions of the P_{21} calculation for the 50% scattering case are given in Fig. 6 and 7. The geometry of problem two allows comparisons of flux distributions in cut planes perpendicular to the y axis. Four cross sections, at y = 5, 45, 75 and 95cm are given in Fig. 7. The high quality of the solution is best observed for cross sections far away from the source region, i.e. at y = 75 and y = 95 cm.

2.3 DISCUSSION OF PROBLEM 3

The geometry of problem 3 can be seen in Fig. 8. The overall dimensions of the problem are 60cm x 100cm x 60cm. The source region is a cube of 10cm on a side located at the origin of the coordinate system. The void region is a dog leg shaped duct with a cross section of 10cm x 10cm. The remaining volume is the absorber.

Table 7 and 8 compare spherical harmonic results of order 5, 9 and 21 with the reference solution provided by Kobayashi. A spatial grid of 56x96x56 grid points is applied for all presented calculations. The total number of spatial cells is 301,056 and thus the number of discretization points in phase space is 21, 60 and 291 million points for P_5, P_9 and P_{21} respectively. For both cases the accuracy of the results improves with increasing spherical harmonic order as previously observed for problem 2.

Flux distributions obtained by P_{21} calculations are given in Figs. 8 and 9 for both cases. The figures show that the problem is well resolved in phase space.

CONCLUSIONS

While the benchmark suite challenges the Ardra code in various aspects, many important features of the Ardra code are not examined by the Kobayashi suite. The salient characteristic of the Ardra code is that it offers robust scalable solution methods for neutron and radiation transport problems in complex 3d geometries. High resolution in space, energy and direction are supported. Ardra has demonstrated its capability to solve systems with billions of unknowns on tera-scale computers with 1000's of processors. The shielding calculation described in (Brown, 2000) simulated the neutron flux coming from a target chamber at LLNL. Over 900 separate surfaces were present in the physical problem specification. In this calculation, 14 orders of magnitude change in the physical properties and 4 orders of magnitude difference in the physical sizes needed to be modeled. The calculation utilized 1,248 nodes (logical 3D node layout: 8 x 12 x 13) of the ASCI Blue SST machine with 4 processors on each node to give a total of 4,992 processors. The domain was decomposed into 150,508,800 total spatial zones (536 x 540 x 520) and 46 energy groups. A first order (in direction) approximation to the scattering kernel was used, which required solution for four unknown moments. A S_6 approximation was used to discretize the direction, which results in 48 quadrature points. This decomposition resulted in over 27 billion unknowns with over 332 billion discretization points. The run required 4 hours of compute time.

ACKNOWLEDGEMENTS

This work was performed under the auspices of the U.S. Department of Energy by the Lawrence Livermore National Laboratory under Contract W-7405-Eng-48.

REFERENCES

1. P.N. Brown, B. Chang, M.R. Dorr, U.R. Hanebutte and C.S. Woodward, Performing Three-Dimensional Neutral Particle Transport Calculations on Tera Scale Computers. High Performance Computing '99 (part of the 1999 Advanced Simulation Technologies Conference), April 11 - 15, 1999, San Diego, CA. Also available as LLNL Technical Report UCRL-JC-132006.

2. P.N. Brown, B. Chang, U.R.Hanebutte and C.S. Woodward, The Quest for a High Performance Boltzmann Transport Solver, (paper accepted for publication and presentation) Sixth International Conference on Applications of High-Performance Computers in Engineering (HPC2000), January 26-28, 2000, Maui, Hawaii. Also available as LLNL Technical Report UCRL-JC-135151.

3. Lawrence Livermore National Laboratory www document IBM Delivers Phase 1 of Blue-Pacific SST to Livermore http://www.llnl.gov/asci/news/phase1_SST.html, October, 3, 1998.

4. K.A. Kobayashi, Proposal for 3D Radiation Transport Benchmarks for Simple Geometries with Void Region. 3-D Deterministic Radiation Transport Computer Programs, OECD/NEA Proceedings, pp. 403 - 410, 1997.

5. N. Sugimura and K.A. Kobayashi, Prelimary Report on 3D Radiation Transport Benchmarks for Simple Geometires with Void Region, Private communication, 1999.

Table I: Cross section and Source Data

Region	Source ($n\ cm^{-3}\ s^{-1}$)	Total Cross Section (cm^{-1})	Scattering Cross Section (cm^{-1}) Problem i	Scattering Cross Section (cm^{-1}) Problem ii
Source	1	0.1	0	0.05
Void	0	10^{-4}	0	$0.5x10^{-4}$
Absorber	0	0.1	0	0.05

Table II: Performance Data for P_{21} Calculations on ASCI Blue Pacific CTR Machine

Problem		**Nodes**	**Proc.'s**	**Number of Iterations**	**Residual Norm**	**Solution Time (Seconds)**
1i	50x50x50 grid	50	200	28	9.718194e-06	7,847
1ii	50x50x50 grid	50	200	38	6.548358e-06	10,223
2i	56x96x56 grid	128	512	79	2.689473e-07	21,115
2ii	56x96x56 grid	64	256	13	8.820067e-06	6,463
3i	56x96x56 grid	64	256	26	9.943451e-07	12,876
3ii	56x96x56 grid	64	256	11	8.184714e-06	5,592

Table III: Problem 1i (pure absorber) on a 50x50x50 grid

	Reference:			Ardra	
	Kyoto	P21		S18	
in y direction at x = z = 5cm			rel error		rel error
5	5.96E-00	5.77E-00	-3.2%	5.94E-00	-0.3%
15	1.37E-00	1.63E-00	18.3%	1.39E-00	1.2%
25	5.01E-01	4.46E-01	-11.0%	5.21E-01	4.0%
35	2.52E-01	2.92E-01	15.7%	2.67E-01	5.8%
45	1.50E-01	1.60E-01	6.2%	8.88E-02	-40.9%
55	5.95E-02	6.69E-02	12.4%	2.88E-02	-51.6%
65	1.53E-02	1.71E-02	11.3%	1.34E-02	-12.6%
75	4.18E-03	3.33E-03	-20.2%	4.92E-03	17.8%
85	1.19E-03	7.44E-04	-37.2%	1.65E-03	39.2%
95	3.47E-04	3.22E-05	-90.7%	7.77E-04	124.0%
diagonal at x = z = z					
5	5.96E-00	5.77E-00	-3.2%	5.94E-00	-0.3%
15	4.71E-01	4.67E-01	-0.7%	4.21E-01	-10.6%
25	1.70E-01	1.67E-01	-1.7%	2.06E-01	21.2%
35	8.68E-02	8.25E-02	-4.9%	5.52E-02	-36.4%
45	5.25E-02	5.57E-02	6.0%	4.11E-02	-21.7%
55	1.33E-02	1.21E-02	-9.6%	2.23E-02	67.2%
65	1.46E-03	1.49E-03	2.0%	3.10E-03	112.5%
75	1.75E-04	1.80E-04	2.7%	3.64E-04	107.6%
85	2.25E-05	2.33E-05	3.8%	7.10E-06	-68.4%
95	3.01E-06	3.15E-06	4.8%	-7.98E-06	-365.1%
in x direction at y = 95cm and z = 5cm					
5	5.95E-02	6.69E-02	12.4%	2.88E-02	-51.6%
15	5.50E-02	6.47E-02	17.6%	5.31E-02	-3.5%
25	4.81E-02	5.01E-02	4.2%	3.46E-02	-28.0%
35	3.97E-02	3.46E-02	-12.8%	3.74E-02	-5.7%
45	3.16E-02	2.95E-02	-6.7%	3.20E-02	1.1%
55	2.35E-02	2.44E-02	3.8%	3.39E-02	44.1%
65	5.84E-03	5.27E-03	-9.7%	6.74E-03	15.5%
75	1.57E-03	1.32E-03	-15.6%	2.39E-03	52.5%
85	4.53E-04	4.66E-04	2.9%	4.39E-04	-3.1%
95	1.37E-04	1.07E-04	-21.8%	-6.28E-05	-100.0%

Table IV: Problem 1ii (50% scattering)

	Reference:	Ardra			
	Monte Carlo	P21		P5	
		50x50x50 grid		150x150x150 grid	
in y direction at x = z = 5cm			rel error		rel error
5	8.29E-00	7.94E-00	-4.1%	4.79E-00	-42.2%
15	1.87E-00	2.18E-00	16.3%	1.45E-00	-22.5%
25	7.13E-01	6.45E-01	-9.5%	1.16E-00	62.7%
35	3.86E-01	4.30E-01	11.5%	8.12E-01	110.6%
45	2.54E-01	2.62E-01	3.0%	4.67E-01	83.6%
55	1.37E-01	1.46E-01	6.5%	1.90E-01	38.2%
65	4.66E-02	4.84E-02	3.7%	6.14E-02	31.6%
75	1.58E-02	1.54E-02	-2.0%	2.09E-02	32.6%
85	5.49E-03	5.08E-03	-7.6%	7.25E-03	32.0%
95	1.83E-03	1.24E-03	-32.1%	2.47E-03	34.7%
diagonal at x = z = z					
5	8.29E-00	7.94E-00	-4.1%	4.79E-00	-42.2%
15	6.64E-01	6.43E-01	-3.3%	1.15E-00	73.1%
25	2.69E-01	2.58E-01	-4.1%	5.17E-01	92.0%
35	1.56E-01	1.51E-01	-3.3%	7.91E-02	-49.5%
45	1.05E-01	1.06E-01	1.6%	2.56E-01	144.7%
55	3.03E-02	2.89E-02	-4.4%	3.43E-02	13.3%
65	4.13E-03	4.18E-03	1.3%	4.42E-03	7.1%
75	5.65E-04	5.99E-04	6.1%	5.97E-04	5.7%
85	7.87E-05	8.91E-05	13.2%	8.43E-05	7.1%
95	9.64E-06	1.09E-05	13.4%	1.02E-05	5.8%
in x direction at y = 95cm and z = 5cm					
5	1.37E-01	1.46E-01	6.5%	1.90E-01	38.2%
15	1.28E-01	1.38E-01	8.0%	1.66E-01	29.9%
25	1.13E-01	1.15E-01	1.7%	1.33E-01	17.2%
35	9.60E-02	9.18E-02	-4.4%	1.12E-01	16.7%
45	7.75E-02	7.67E-02	-1.1%	9.85E-02	27.1%
55	5.66E-02	5.74E-02	1.5%	6.85E-02	21.1%
65	1.89E-02	1.89E-02	0.0%	2.42E-02	28.3%
75	6.40E-03	6.68E-03	4.4%	8.40E-03	31.3%
85	2.33E-03	2.28E-03	-1.9%	3.01E-03	29.2%
95	7.94E-04	7.24E-04	-8.9%	1.05E-03	32.2%

Table V: Problem 2i (pure absorber) on a 56x96x56 grid

	Reference: Kyoto	P5		Ardra P9		P21	
in y direction at x = z = 5cm			rel error		rel error		rel error
5	5.96E-00	5.71E-00	-4.1%	5.89E-00	-1.1%	5.96E-00	0.1%
15	1.37E-00	1.32E-00	-3.8%	1.31E-00	-4.5%	1.32E-00	-3.8%
25	5.01E-01	2.33E-01	-53.5%	4.63E-01	-7.6%	4.96E-01	-1.0%
35	2.52E-01	1.66E-01	-34.2%	1.95E-01	-22.8%	2.58E-01	2.2%
45	1.50E-01	1.22E-01	-18.8%	8.93E-02	-40.6%	1.48E-01	-1.5%
55	9.92E-02	1.00E-01	0.8%	7.93E-02	-20.0%	9.94E-02	0.2%
65	7.02E-02	6.79E-02	-3.2%	6.90E-02	-1.7%	7.18E-02	2.3%
75	5.22E-02	8.01E-02	53.4%	7.94E-02	52.1%	4.72E-02	-9.6%
85	4.03E-02	1.06E-01	162.9%	5.62E-02	39.4%	3.46E-02	-14.2%
95	3.21E-02	8.28E-02	158.3%	3.31E-02	3.3%	2.86E-02	-10.8%
in x direction at y = 95cm and z = 5cm							
5	3.21E-02	8.28E-02	158.3%	3.31E-02	3.3%	2.86E-02	-10.6%
15	1.71E-03	6.38E-05	-96.3%	3.54E-03	107.6%	1.85E-03	8.4%
25	1.41E-04	7.69E-04	447.1%	6.65E-04	373.1%	1.80E-06	-98.7%
35	3.27E-05	9.30E-05	184.4%	1.49E-04	355.6%	4.66E-05	42.4%
45	1.09E-05	1.94E-05	78.8%	-1.25E-05	-215.2%	1.21E-05	11.3%
55	4.14E-06	8.19E-06	97.8%	-3.91E-05	-1044.1%	1.97E-05	376.2%

Table VI: Problem 2ii (50% scattering) on a 56x96x56 grid

	Reference: Monte Carlo	P5		Ardra P9		P21	
in y direction at x = z = 5cm			rel error		rel error		rel error
5	8.61E-00	8.10E-00	-5.9%	8.46E-00	-1.7%	8.61E-00	0.0%
15	2.16E-00	2.04E-00	-5.6%	2.06E-00	-4.7%	2.13E-00	-1.5%
25	8.94E-01	5.26E-01	-41.1%	8.35E-01	-6.6%	8.87E-01	-0.7%
35	4.78E-01	3.48E-01	-27.2%	4.01E-01	-16.1%	4.77E-01	-0.1%
45	2.89E-01	2.34E-01	-19.0%	2.16E-01	-25.2%	2.93E-01	1.5%
55	1.89E-01	1.85E-01	-1.9%	1.62E-01	-14.1%	2.06E-01	9.2%
65	1.31E-01	1.48E-01	13.3%	1.28E-01	-2.0%	1.48E-01	13.1%
75	9.49E-02	1.53E-01	61.2%	1.25E-01	31.7%	7.93E-02	-16.5%
85	7.10E-02	1.75E-01	146.3%	9.06E-02	27.5%	4.92E-02	-30.7%
95	5.46E-02	1.30E-01	138.0%	5.89E-02	7.8%	3.66E-02	-33.0%
in x direction at y = 95cm and z = 5cm							
5	5.46E-02	1.30E-01	138.0%	5.89E-02	7.8%	3.66E-02	-33.0%
15	6.63E-03	5.52E-03	-16.7%	8.91E-03	34.4%	7.65E-03	15.3%
25	1.27E-03	2.74E-03	115.0%	2.14E-03	67.9%	1.20E-03	-5.5%
35	4.19E-04	6.22E-04	48.4%	6.25E-04	49.1%	3.52E-04	-16.1%
45	1.74E-04	2.29E-04	31.5%	1.58E-04	-9.3%	1.56E-04	-10.7%
55	5.92E-05	7.48E-05	26.3%	1.96E-05	-66.9%	5.08E-05	-14.3%

Table VII: Problem 3i (pure absorber) on a 56x96x56 grid

	Reference: Kyoto	P5		Ardra P9		P21	
in y direction at x = z = 5cm			rel error		rel error		rel error
5	5.96E-00	5.72E-00	-4.0%	5.91E-00	-0.8%	5.96E-00	0.1%
15	1.37E-00	1.36E-00	-1.0%	1.35E-00	-1.6%	1.34E-00	-2.3%
25	5.01E-01	2.92E-01	-41.7%	4.89E-01	-2.4%	4.95E-01	-1.2%
35	2.52E-01	2.09E-01	-17.2%	2.22E-01	-12.1%	2.49E-01	-1.4%
45	1.50E-01	1.87E-01	24.6%	9.97E-02	-33.6%	1.56E-01	3.9%
55	9.92E-02	1.21E-01	21.8%	8.54E-02	-13.9%	1.20E-01	21.4%
65	4.23E-02	4.41E-02	4.3%	5.41E-02	28.0%	5.10E-02	20.7%
75	1.15E-02	1.64E-02	42.9%	1.27E-02	10.7%	8.91E-03	-22.4%
85	3.25E-03	4.69E-03	44.4%	3.33E-03	2.6%	1.95E-03	-39.9%
95	9.48E-04	1.32E-03	38.9%	1.13E-03	19.2%	6.82E-04	-28.1%
in x direction at y = 55cm and z = 5cm							
5	9.92E-02	1.21E-01	21.8%	8.54E-02	-13.9%	1.20E-01	21.4%
15	2.45E-02	1.36E-02	-44.4%	1.53E-02	-37.6%	2.24E-02	-8.7%
25	4.54E-03	1.77E-02	289.2%	2.18E-03	-52.0%	3.80E-03	-16.4%
35	1.43E-03	1.43E-02	903.1%	4.40E-03	207.8%	9.80E-04	-31.4%
45	2.65E-04	1.21E-03	357.6%	1.54E-03	481.5%	2.14E-04	-19.4%
55	9.14E-05	4.29E-04	369.7%	3.88E-04	324.4%	1.46E-04	59.4%
in x direction at y = 95cm and z = 35 cm							
5	3.27E-05	3.01E-05	-8.0%	2.91E-05	-11.0%	2.20E-05	-32.9%
15	2.68E-05	2.66E-05	-0.9%	2.77E-05	3.2%	2.36E-05	-12.1%
25	1.70E-05	5.32E-06	-68.7%	1.25E-05	-26.5%	1.59E-05	-6.2%
35	3.38E-05	5.48E-05	62.1%	3.71E-05	9.8%	2.86E-05	-15.3%
45	6.05E-06	7.47E-06	23.6%	7.40E-06	22.3%	6.32E-06	-4.4%
55	3.36E-06	4.42E-07	-86.9%	-8.87E-08	-102.6%	3.44E-06	2.4%

Table VIII: Problem 3ii (50% scattering) on a 56x96x56 grid

	Reference:			Ardra			
	Monte Carlo	P5		P9		P21	
in y direction at x = z = 5cm			rel error		rel error		rel error
5	8.60E-00	8.14E-00	-5.4%	8.51E-00	-1.1%	8.61E-00	0.1%
15	2.16E-00	2.11E-00	-2.5%	2.12E-00	-2.1%	2.13E-00	-1.7%
25	8.93E-01	6.21E-01	-30.5%	8.72E-01	-2.3%	8.84E-01	-1.0%
35	4.77E-01	4.18E-01	-12.4%	4.43E-01	-7.2%	4.72E-01	-1.0%
45	2.89E-01	3.39E-01	17.2%	2.29E-01	-20.8%	2.99E-01	3.4%
55	1.93E-01	2.24E-01	16.2%	1.77E-01	-8.2%	2.24E-01	16.1%
65	1.05E-01	1.15E-01	9.3%	1.21E-01	15.0%	1.19E-01	13.0%
75	3.39E-02	4.38E-02	29.1%	3.53E-02	4.1%	3.02E-02	-11.1%
85	1.08E-02	1.42E-02	31.4%	1.08E-02	-0.1%	8.54E-03	-21.0%
95	3.48E-03	4.37E-03	25.7%	3.57E-03	2.7%	2.83E-03	-18.5%
in x direction at y = 55cm and z = 5cm							
5	1.93E-01	2.24E-01	16.2%	1.77E-01	-8.2%	2.24E-01	16.1%
15	6.75E-02	5.61E-02	-16.8%	5.74E-02	-14.9%	6.42E-02	-4.9%
25	2.23E-02	4.15E-02	86.5%	1.93E-02	-13.3%	2.03E-02	-8.9%
35	9.95E-03	2.88E-02	189.5%	1.46E-02	46.8%	1.00E-02	1.0%
45	3.37E-03	5.78E-03	71.4%	5.70E-03	69.0%	3.41E-03	1.0%
55	1.05E-03	2.03E-03	93.7%	1.60E-03	52.7%	1.17E-03	11.2%
in x direction at y = 95cm and z = 35 cm							
5	3.34E-04	3.50E-04	4.7%	3.35E-04	0.2%	3.17E-04	-5.3%
15	2.82E-04	2.84E-04	0.6%	2.86E-04	1.3%	2.78E-04	-1.3%
25	2.03E-04	1.81E-04	-10.7%	1.94E-04	-4.3%	2.00E-04	-1.2%
35	2.46E-04	3.27E-04	33.0%	2.64E-04	7.3%	2.55E-04	3.7%
45	1.15E-04	1.03E-04	-10.8%	1.08E-04	-6.5%	1.07E-04	-7.4%
55	3.37E-05	3.84E-05	14.0%	4.11E-05	22.0%	4.50E-05	33.7%

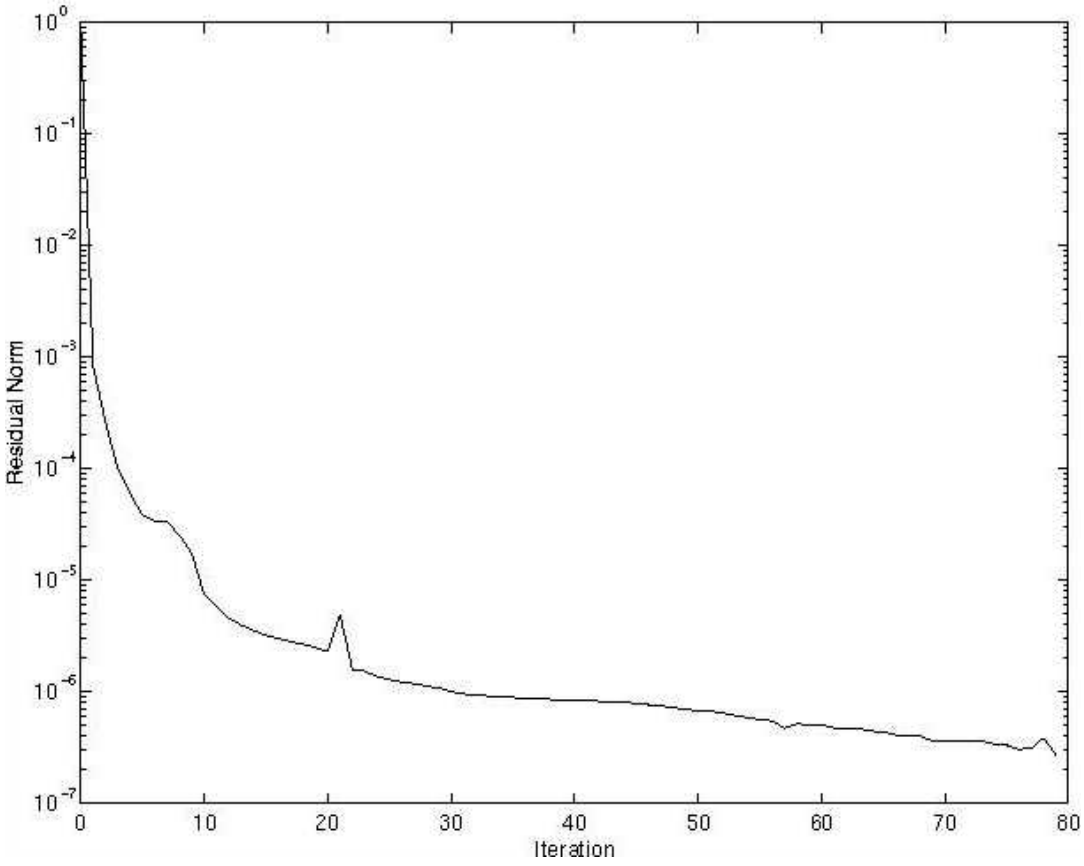

Figure 1: Convergence: Problem 2i (pure absorber), P_{21} solution on 56x96x56 spatial grid.

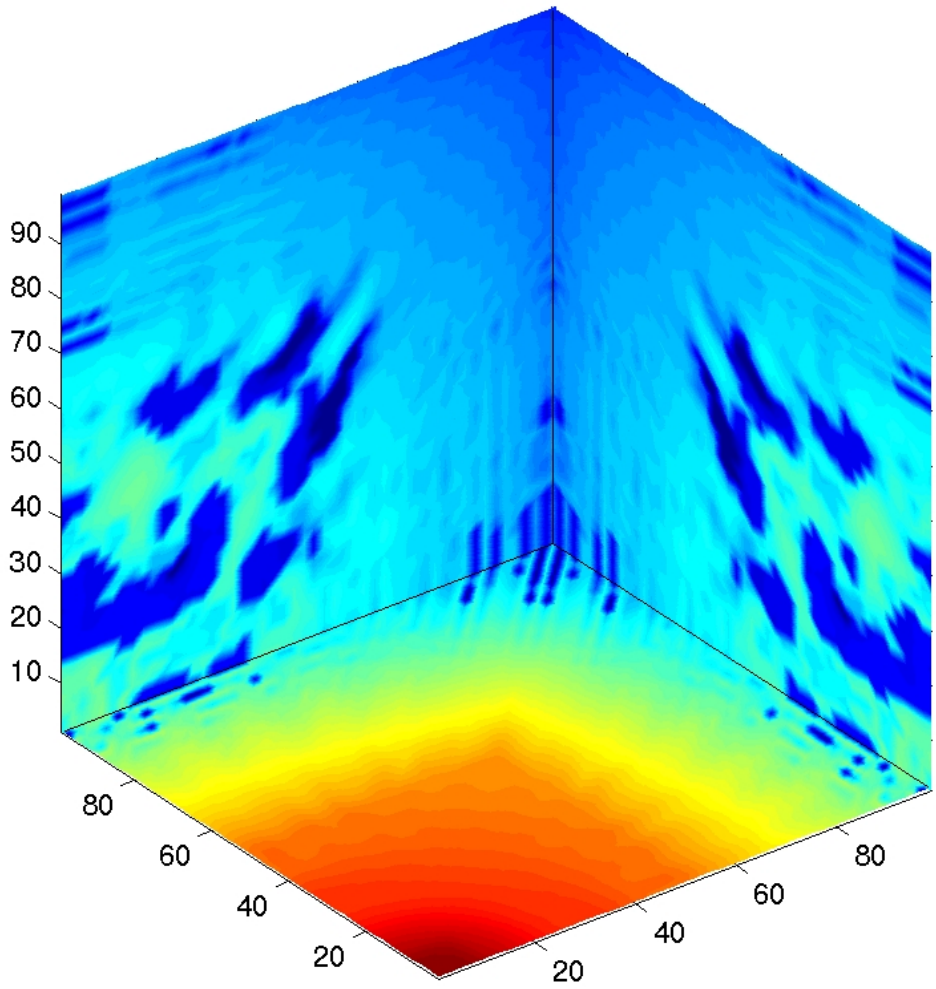

Figure 2: Scalar Flux: Problem 1i (pure absorber), P_{21} solution on a 50x50x50 spatial grid.

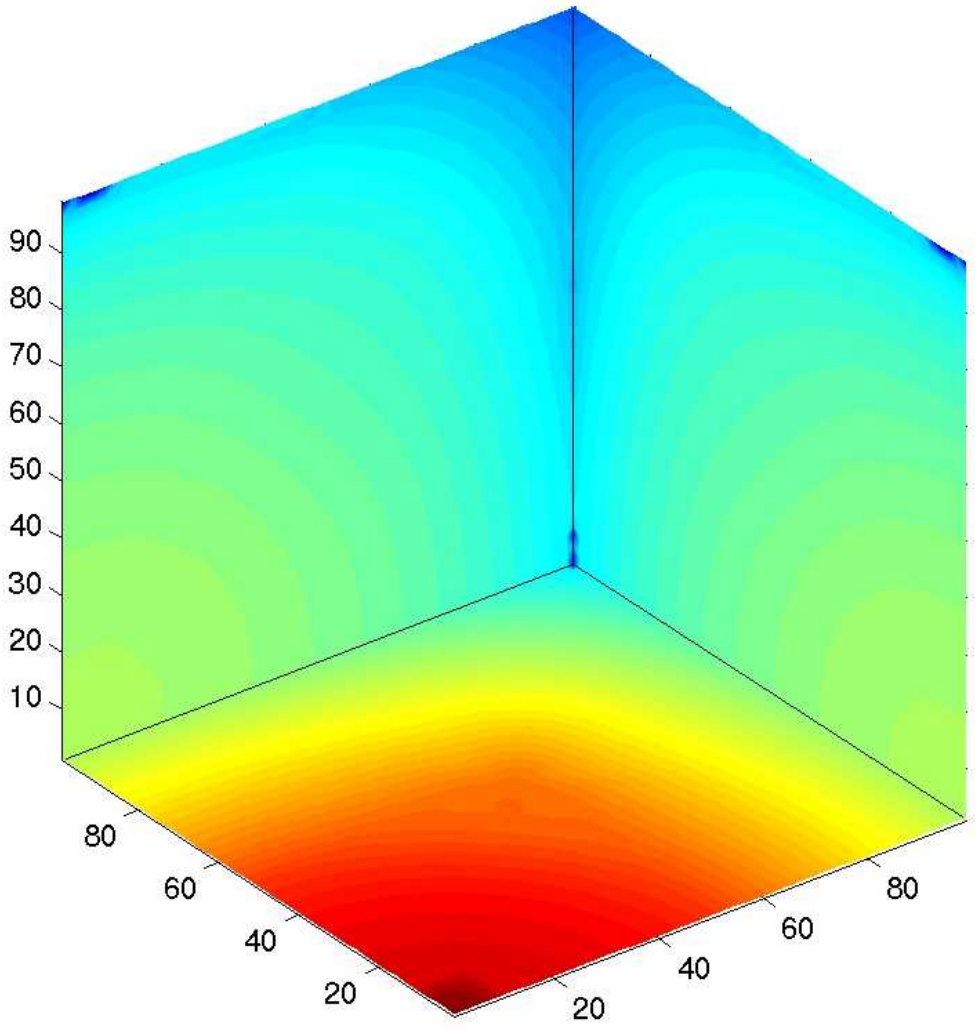

Figure 3: Scalar Flux: Problem 1ii (50% scattering), P_5 solution on a 150x150x150 spatial grid.

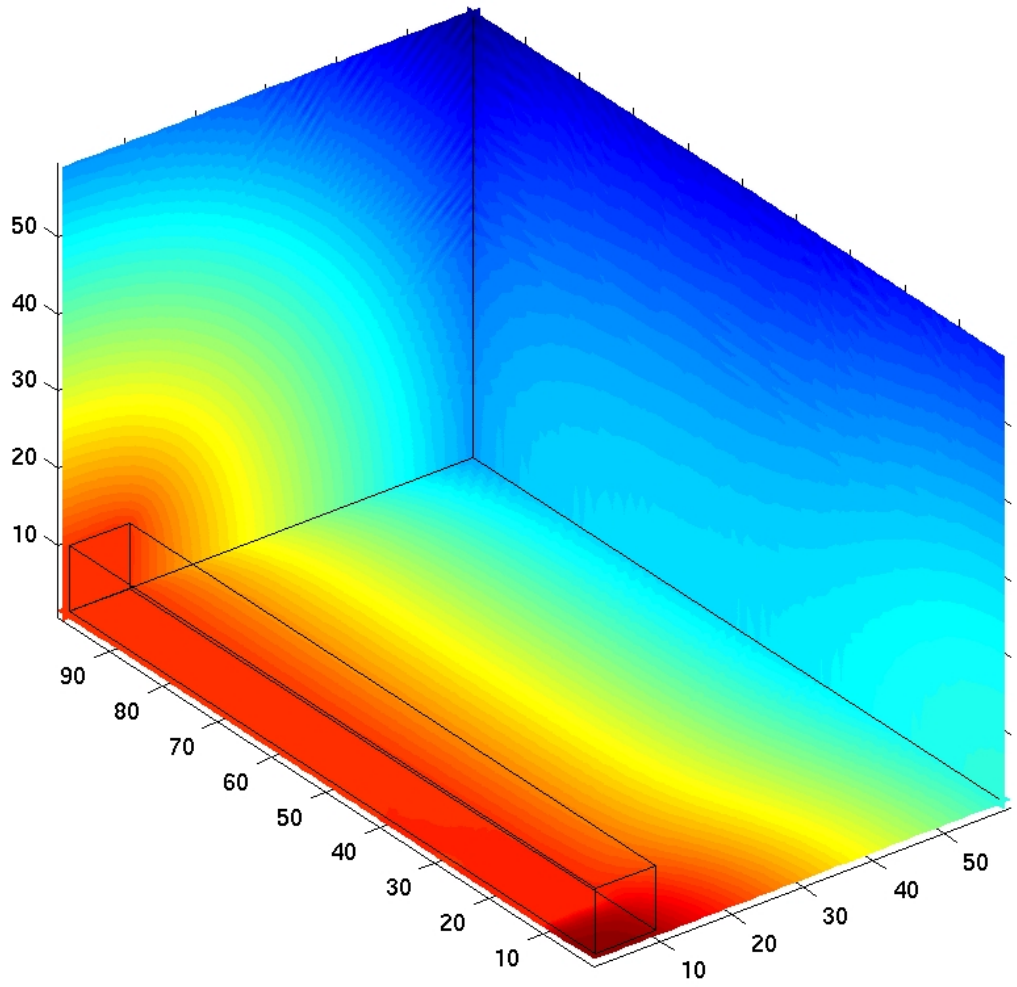

Figure 4: Scalar Flux: Problem 2i (pure absorber), P_1 solution (i.e. diffusion approximation) on a 56x96x56 spatial grid.

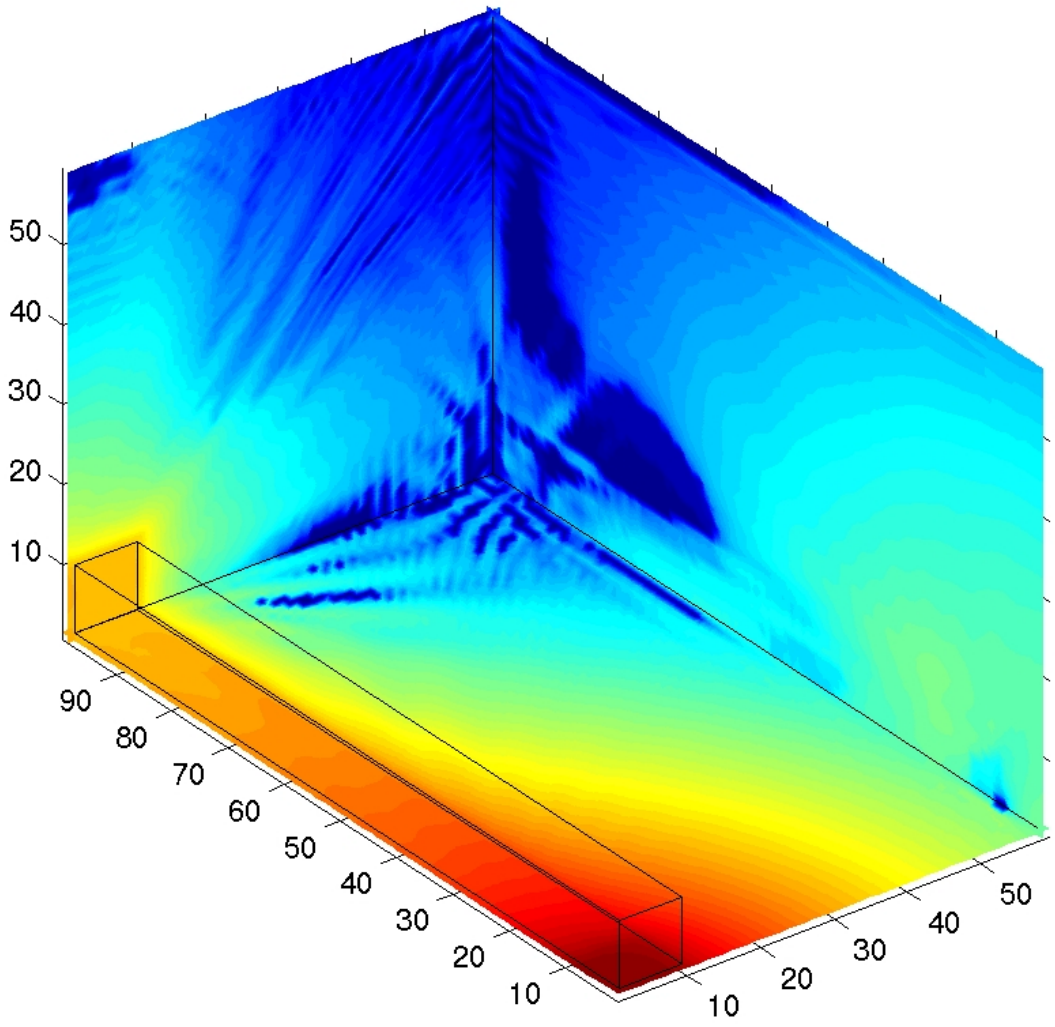

Figure 5: Scalar Flux: Problem 2i (pure absorber), P_{21} solution on a 56x96x56 spatiale grid.

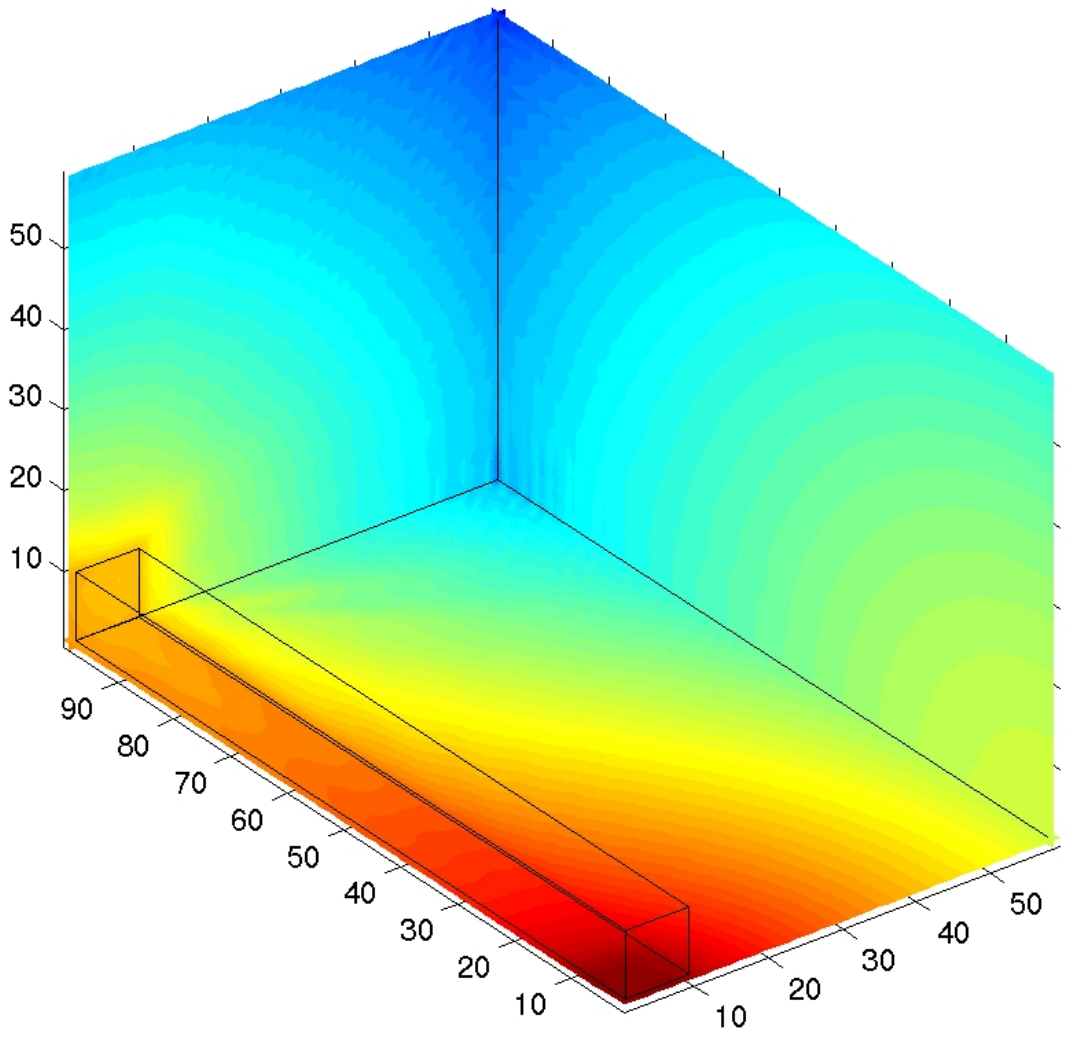

Figure 6: Scalar Flux: Problem 2ii (50% scattering), P_{21} solution on a 56x96x56 spatial grid.

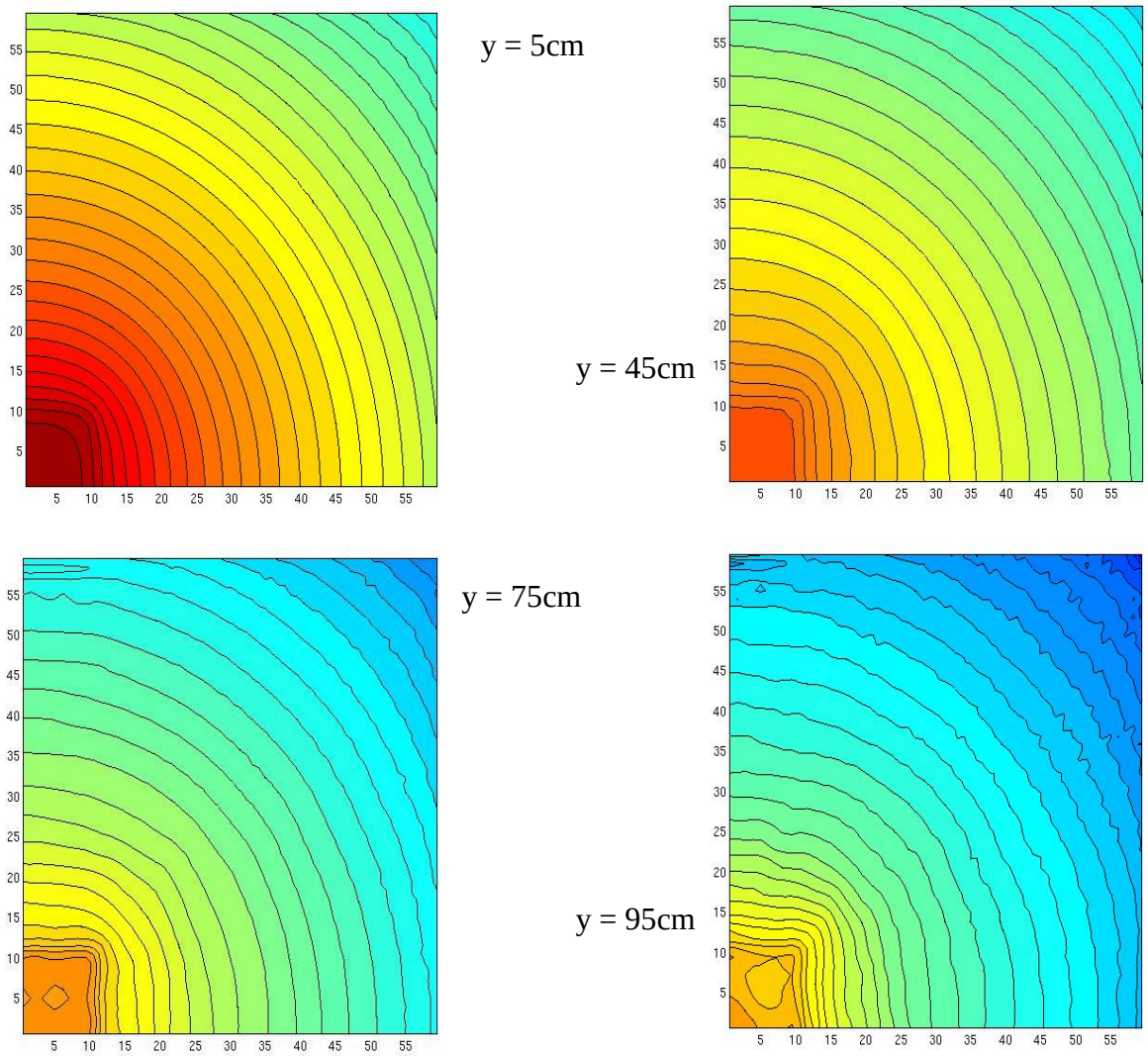

Figure 7: Scalar flux: Problem 2ii (50% scattering) P_{21} solution on a 56x96x56 spatial grid. Cross sections at y = 5, 45, 75 and 95 cm.

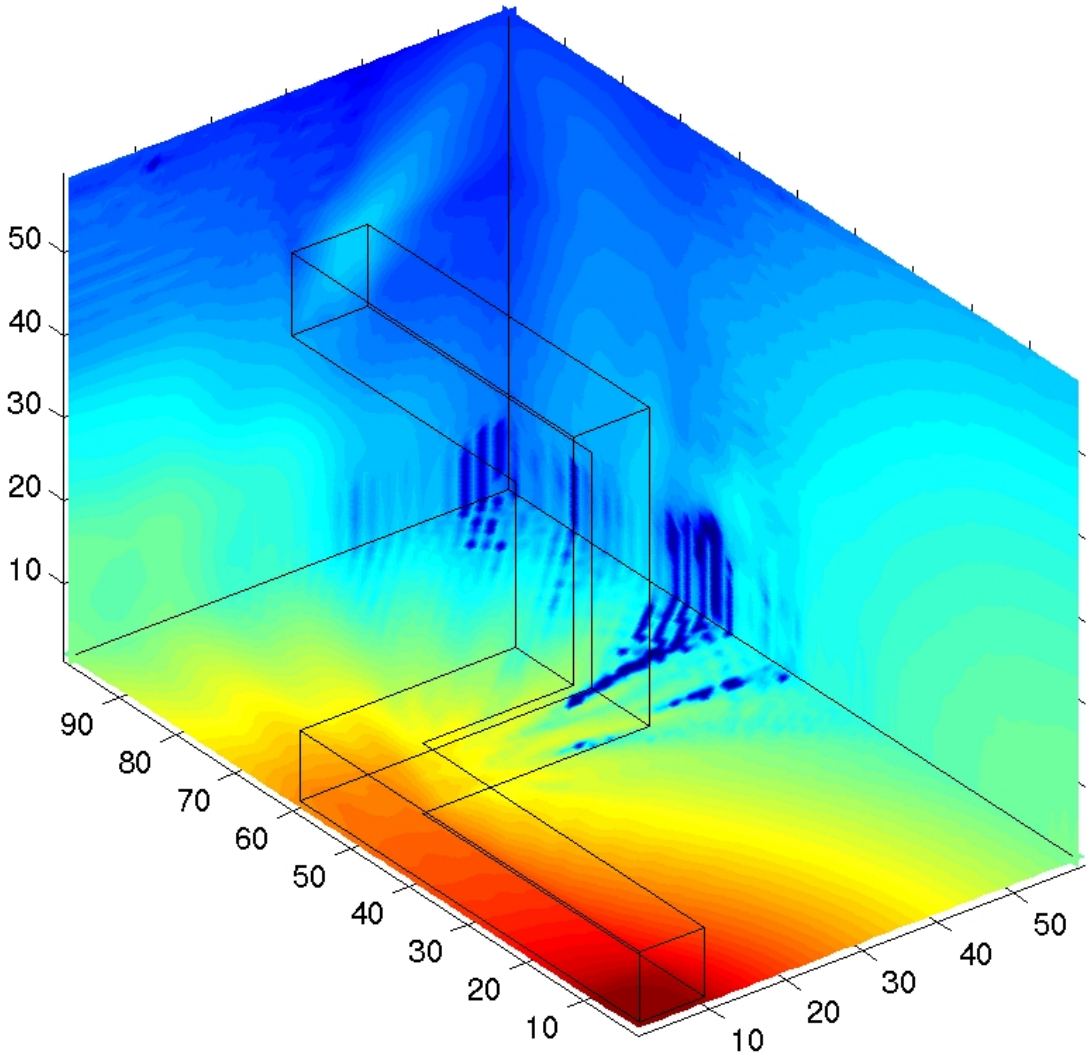

Figure 8: Scalar Flux: Problem 3i (pure absorber), P_{21} solution on a 56x96x56 spatial grid.

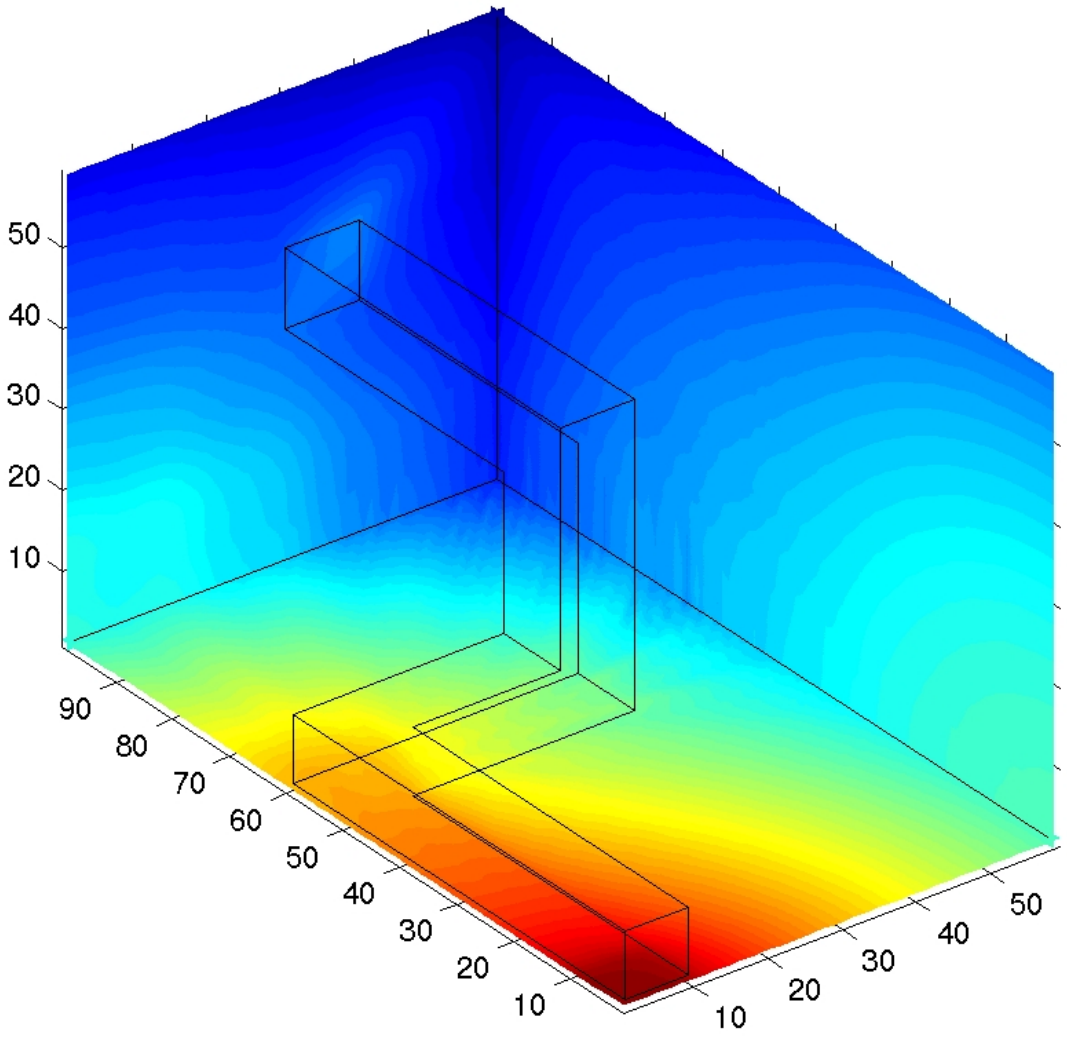

Figure 9: Scalar Flux: Problem 3ii (50% scattering), P_{21} solution on a 56x96x56 spatial grid.